IEEE Access
Multidisciplinary | Rapid Review | Open Access Journal

Received February 28, 2019, accepted May 5, 2019, date of publication June 13, 2019, date of current version July 15, 2019.

Digital Object Identifier 10.1109/ACCESS.2019.2922383

Practical Control Strategy for Positioning Control of Pneumatic Artificial Muscles Driven Stage: Improved NCTF Control

T. F. TANG[1], (Student Member, IEEE), S.-H. CHONG[1], (Senior Member, IEEE), R. MOHD NOR[2], AND KAIJI SATO[3], (Senior Member, IEEE)

[1]Centre for Robotics and Industrial Automation, Faculty of Electrical Engineering, Universiti Teknikal Malaysia Melaka, Melaka 76100, Malaysia
[2]Department of Electrical Technology, Faculty of Engineering Technology, Universiti Teknikal Malaysia Melaka, Melaka 76100, Malaysia
[3]Department of Mechanical Engineering, Toyohashi University of Technology, Toyohashi 441-8580, Japan

Corresponding author: S.-H. Chong (horng@utem.edu.my)

This work was supported in part by the University Short Term Research under Grant PJP/2018/FTK(17C)/S01643 and in part by the scholarship of Skim Zamalah from Universiti Teknikal Malaysia Melaka.

ABSTRACT This paper presents a practical control strategy for motion control of a pneumatic muscle actuated the system. Pneumatic artificial muscle (PAM) exhibits strong nonlinear characteristics which are difficult to be modeled precisely, and these characteristics have led to low controllability and difficult to achieve high precision control performance. This paper aims to propose nominal characteristic trajectory following (NCTF) control system, which emphasizes simple design procedure without the need of exact model parameters, and yet is able to demonstrate high performance in both point-to-point and continuous motions. However, the conventional NCTF controller does not offer a promising positioning performance with the PAM mechanisms, where it exhibits large vibration in the steady state before the mechanism stopping and tends to reduce the motion accuracy. Therefore, the objective of this study is to improve the conventional NCTF controller by removing the actual velocity feedback to eliminate vibration problem, added an acceleration feedback compensator to the plant model, and a reference rate feedforward to solve low damping characteristic of the PAM mechanism simultaneously improve tracking following characteristic. The design procedure of the improved NCTF controller remains easy and straightforward. The effectiveness of the proposed controller is verified experimentally and compared with the conventional NCTF and classical PI controllers in the performances of positioning and continuous motion. The improved NCTF controller reduces the positioning error up to 90% and 63% as benchmarked to the PI and conventional NCTF controllers, respectively, while it reduces up to 92% (PI) and 95% (NCTF) in the tracking error.

INDEX TERMS Motion control, NCTF control, nonlinear system, pneumatic artificial muscle, practical controller.

I. INTRODUCTION

In the year of 1950, McKibben pneumatic artificial muscle was originally invented by J. L. McKibben [1]. Pneumatic artificial muscle (PAM) is a unique unidirectional actuator, which has merely similar force-contraction profiles as the skeletal muscle. Both PAM and skeletal muscle exhibit similar macroscopic shape change when activated. The PAM is made by an expandable rubber tube, and the rubber tube is surrounded by an inextensible braided shell. The rubber tube is increasing in volume when the pressurized air is supply. Due to the inextensibility of the braided shell, it limits the rubber tube to enlarge in radius but shortens axially. When depressurized, the PAM returns passively. Thus, the PAM has only one active action where it contracts via pressurized air to exert a pulling force.

As compared to conventional actuators, the PAM has simpler structure, lighter weight, higher power-to-weight ratio and higher safety in use. Owing to these factors, the PAM has been widely used in the power assist devices [2]–[5],

The associate editor coordinating the review of this manuscript and approving it for publication was Bo Shen.

biomimetic robot [6]–[10], medical applications [11], industry machinery [12], [13] and so on. However, the PAM system exhibits significant nonlinear characteristics such as hysteresis, low damping ability and creep phenomenon, which are caused by the air compressibility, the internal friction and the deformation of the elastic tube. The condition of low damping ability of PAM mechanism will consequently result in pressure response delay and oscillatory motion. These limitations are restricted the applications of the PAM in high precision control system because of its low controllability. Hence, it is challenging to achieve the high speed and high accuracy motion of the PAM system. To further extend the applications of the PAM, an enhancement of its positioning accuracy is required.

To deal with the nonlinearity of PAM mechanism, a proportional-integral-derivative (PID) controller was incorporated with the feedforward hysteresis compensation that describes the static hysteresis behavior of the PAM mechanism [14], [15]. However, the static hysteresis compensator is not robust enough to compensate the nonlinearity and does not offer a promising performance in the higher tracking frequency. Over the years, nonlinear model-based control approaches, such as sliding mode control (SMC) [16]–[19], backstepping control [20], [21], saturated adaptive robust control [22], switching model predictive control [23], and variable structure control [24] have become another important solutions to achieve high positioning performance for PAM systems. Aschemann and Schindele [16] have successfully proposed SMC including a nonlinear disturbance observer for a high speed linear axis driven by pneumatic muscles actuated system. The best tracking accuracy achieved is on the order of 3.5 mm. In the same year, the same team has designed a backstepping control for the same experimental setup, and the best tracking accuracy reported was smaller than 0.2 mm [21]. In [18], Cao and his team have realized a new MIMO SMC on a PAM actuated robotic mechanism that of for rehabilitation purpose. They examined the control performance of the joint angular trajectory by varying different input frequencies and reported that the highest trajectory accuracy was 3.11°. In fact, the performances of these controllers are relying on the accuracy of the identified model and its parameters.

To solve the problem of the unmodeled or unknown parameters in the model-based control, various learning intelligent controls were proposed to fine-tune the control parameters, such as advanced intelligent nonlinear PID control [25], [26], fuzzy PD+I control [27], adaptive fuzzy SMC [28]–[30], hybrid fuzzy-neural control [31] and switching predictive approaches [32]. The intelligent control with learning capability provides satisfied positioning performance. However, the nonlinear models are required for this controller as well. Also, the controller design is complex and requires sufficient knowledge of the intelligent algorithms. Many good control approaches have been stated in the literature, they demonstrate a good performance for the PAM mechanism. However, they have a similar issue, which they have complex control structure and complicated design procedure. In the industry, those controllers are impracticable for the engineers who have inadequate knowledge of the control theory. In year 2013, Woods and his team [33] have proposed a control approach that requires no system model and no prior information about the desired command signal for an active rotor system that driven by the PAMs. This practical control strategy was evaluated, and a promising tracking performance was shown especially in high speed performance. Overall, the output has given good impact in the field of PAM, and it has encouraged us to further investigate the usefulness of the PAM system in achieving better accuracy performance of PAM system, especially in small working range.

Nominal characteristic trajectory following (NCTF) control is a practical control method that highlights a simple control structure and straightforward design procedure, and yet it offers a promising positioning performance. The advantage of this controller is that the design procedure does not need the exact model parameters. The objective of this present study is to improve the NCTF control for a pneumatic muscle actuated system in order to achieve high positioning control. As such, a practical design procedure of the improved NCTF control is determined in reference to the conventional one. In the past three decades, the NCTF control has been improved to be useful in wider applications in industry, where they are the NCTF control, Continuous Motion NCTF control and Acceleration-Reference Continuous Motion NCTF control [34]. The performances of the NCTF control systems have been examined and clarified in various different types of mechanism, such as electric-motor driven typical mechanism with friction [35]–[39], non-contact mechanism [40]–[42], and pneumatic actuator [43]. In achieving high positioning control performance of a PAM system, the conventional NCTF controller suffers of less positioning accuracy and low following characteristic in tracking motion. In addition, the conventional NCTF control system tends to exhibit vibration in high tracking frequency. Therefore, the conventional NCTF control structure is improved in the reason to enhance positioning accuracy in positioning and tracking motions.

In the next section, the experimental setup that used for the performance evaluation is described. Section III discusses the control concept of the conventional NCTF controller and its problems, then the design procedure of the improved NCTF controller is explained clearly in the following. In Section IV, the comparative results of the positioning and tracking performances between the improved NCTF controller, the conventional NCTF controller and the PI controller are evaluated. Lastly, the conclusion is remarked in Section V.

II. PAM DRIVEN STAGE

Fig. 1 shows an experimental setup. A 2 kg mover is located in between the two pneumatic artificial muscles (PAMs) (FESTO DMSP-10-150N-RM-CM) to construct a linear antagonistic configuration. The two PAMs generate pulling forces to push and pull the mover in the horizontal way with the working range of ±2.4 mm. The motion of both

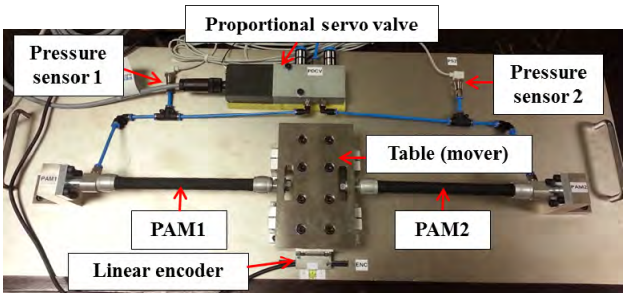

FIGURE 1. PAM driven stage.

the PAMs is governed by a 5/3-way proportional servo valve (FESTO MPYE-5-1/8LF-010-B), and the pressure supply is 0.5 MPa. For monitoring purpose, the pressure of both PAMs is measured by the pressure sensor (SMC PSE540A-01) with the resolution of 0.0012 MPa. To measure the displacement of the mover, a linear encoder (MicroE Systems MII5800-AB-200-5-1-0) with the resolution of 0.1 μm is used as a single feedback sensor in this mechanism. A data acquisition unit is interfaced with a host computer that installed MATLAB/Simulink software for the signal processing. The sampling frequency is 10 kHz (sampling time, $T_s = 0.1$ ms). None of the practical adjustments were made to the experimental system while the control strategies were evaluated.

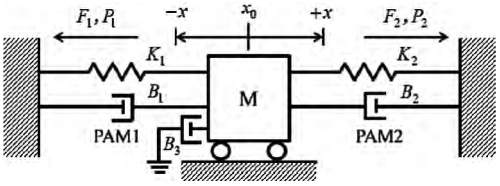

FIGURE 2. Dynamic model of PAM mechanism.

Fig. 2 shows the dynamic model of the PAM mechanism. The middle position of the mover is considered as the initial position. The motion equation of the PAM driven stage can be written as:

$$M\ddot{x} + B\dot{x} + Kx = F_2 - F_1 - F_{friction} \tag{1}$$

where M is the mass of the mover, B is the damping coefficient, and K is the spring coefficient. F_1 and F_2 represent the contractile forces of PAM 1 and PAM 2, respectively. Then, the friction force between the mover and the linear guide is represented as $F_{friction}$. Based on (1), the PAM mechanism is expressed as a third-order system. Due to the high nonlinearity of the PAM mechanism, these make the system model becomes complex and difficult to model it accurately.

Fig. 3(a) shows the normalized experimental open-loop step responses of PAM mechanism under different input voltages with the same pressure supply of 0.5 MPa. The static relationship between the input voltages and the mover is nonlinear. As can be observed in the step responses, the nonlinear characteristics are not significant even though it has

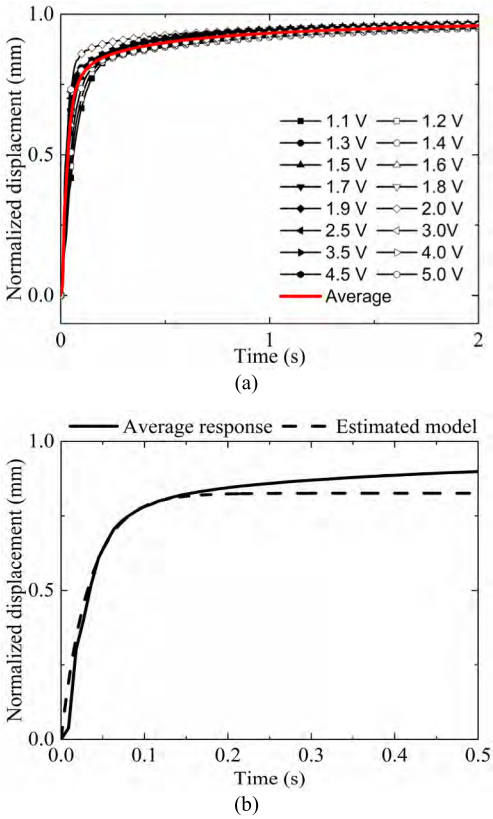

FIGURE 3. (a) Normalized experimental open-loop step responses and an average response; (b) the measured average response and an estimated first-order model.

the nonlinearity dynamic. Also, the measured responses show zero overshoot and nonzero initial slope, where the PAM mechanism is estimated as a first-order system as shown below:

$$G_{plant}(s) = \frac{k}{\tau s + 1} = \frac{0.826}{0.034s + 1} \tag{2}$$

Fig. 3(b) presents the comparison of a measured average response and an approximated first-order model based on (2). The value of the k and τ are determined by approximating the estimated response to the measured average response. The estimated system gain, k and time constant, τ are 0.0826 and 0.034 s respectively. As referred to the Fig. 3(b), the linearized model agrees with the experimental response at the transient response, but not at the steady-state. The creep phenomenon at the final state that found in the averaged experimental results does not agreed with the estimated one. The creep phenomenon can be observed, where the displacement of the mover is increasing at the final state over the time and not stationary at certain position although the constant input voltage is provided. Since the PAM is made from the rubber tube, this phenomenon can occur as a result of long-term exposure to high level of stress that is still below the yield strength of the material. However, the nonlinearity is not significant, and the PAM system can be roughly represented in first-order system.

III. CONTROLLER DESIGN

A. CONVENTIONAL NCTF CONTROL SYSTEM

Nominal characteristic trajectory following (NCTF) controller emphasizes a simple structure and straightforward design procedure without the need of exact model. Fig. 4 presents the control structure of the conventional NCTF control system. The NCTF controller is consist of two elements which are a nominal characteristic trajectory (NCT) and a PI compensator. The NCT is the reference motion trajectory that constructed on phase plane based on the measured actual open-loop response of the mechanism. The function of the NCT is to restrict the motion of the mechanism to follow along the determined trajectory. The deceleration motion of the mechanism in positioning is used to construct the NCT, which this motion is significantly affect the positioning performance with included the friction and saturation effects. As an advantage, the exact model and parameters of the mechanism are not needed to determine the NCT, which makes the design procedure simpler and more straightforward. For PI compensator, it drives the motion of the mechanism to follow the NCT macroscopically and end the motion at the origin of the phase plane. The PI gains are designed using a practical stability limit. The practical stability limit is obtained where the stability of the control system is considered based on the parameters of the measured open-loop responses and the NCT. The detail of the parameters will be explained in Section III.D. In short, the NCT is used to determine the virtual error rate reference, and the PI compensator is used for the velocity control. The control law, u_c of the conventional NCTF controller is expressed in (3).

$$u_c(s) = (\dot{e}_{NCT}(s) - x(s)s)\left(K_p + \frac{K_i}{s}\right) \tag{3}$$

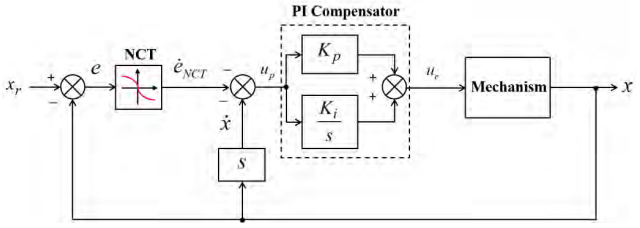

FIGURE 4. Control structure of the conventional NCTF control system. The structure consists of two element which are a nominal characteristic trajectory (NCT) and a PI compensator.

Fig. 5 illustrates the NCT and the plant motion on the phase plane. In the beginning, the PI compensator leads the object motion to reach the trajectory in reaching phase. Then, the following phase takes place after the object motion reached the trajectory. The PI compensator further leads the object motion to the origin of the phase plane. In other words, the PI compensator works for reduction of the difference of the NCT and the actual motion.

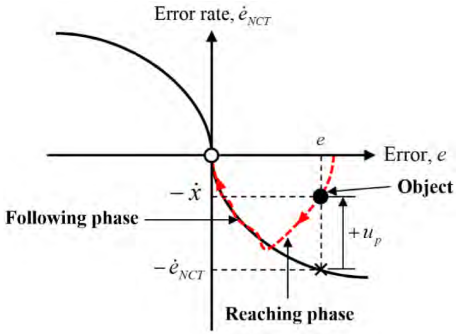

FIGURE 5. Nominal characteristic trajectory (NCT) and the plant motion. The object motion is controlled to reach the trajectory in the reaching phase and then follow the trajectory in the following phase.

B. PROBLEMS OF THE CONVENTIONAL NCTF CONTROLLER TO THE PAM MECHANISM

Fig. 6 shows the experimental positioning performance of the conventional NCTF controller. The responses exhibit the stick-slip phenomenon before stopping, which lead to the large steady-state error with 1.3 μm at 0.1 mm and 10.2 μm at 2 mm. Fig. 7 presents the experimental tracking motion results of the conventional NCTF controller that driven by sinusoidal input signals of 0.1 Hz and 0.1 mm, and 0.3 Hz and 2 mm, respectively. Both tracking results demonstrates low following characteristic to the reference although in low frequency (0.1 Hz) and large tracking error occurred. When the mechanism is commanded by higher frequency (0.3 Hz) in larger working range (2 mm), the PAM control system exhibits vibration and fails to perform in the fast tracking motion as presented in Fig. 7(b).

To solve the problems of the conventional NCTF controller to the PAM mechanism, an improved NCTF controller is proposed to enhance the position accuracy and following characteristic of the system. Based on the conventional NCTF control structure, the improved NCTF controller is designed to fulfill the requirements, where it is able to:

(A) eliminate the vibration in the fast tracking motion.
(B) improve the damping characteristic that is able to reduce the oscillation in the steady-state response.
(C) improve the following characteristic to reduce the tracking error.

C. IMPROVED NCTF CONTROL SYSTEM

Fig. 8 shows the control structure of the improved NCTF controller for the PAM mechanism. To achieve the abovementioned requirements, the improved NCTF control has done the three changes, i.e., removing the actual velocity feedback (pure derivative block), adding an acceleration feedback compensator (double pure derivative blocks) and adding a feedforward of reference rate (pure derivative block).

The working range of the constructed PAM mechanism is considered small, where it is just $\pm$2.4 mm. In this small working range, the effect of the velocity response is

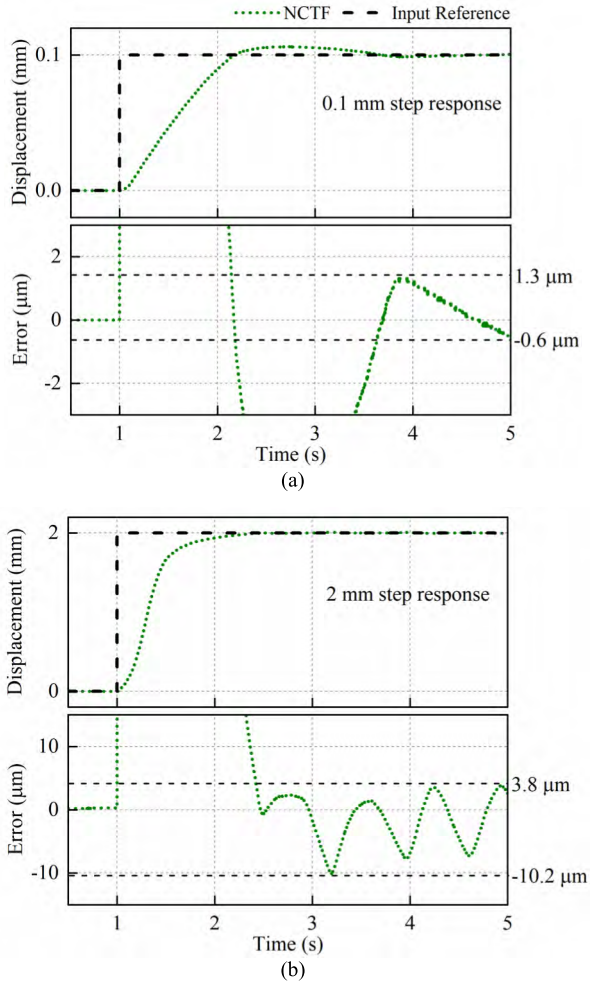

FIGURE 6. Experimental positioning performance of the conventional NCTF controller at (a) 0.1 mm and (b) 2 mm.

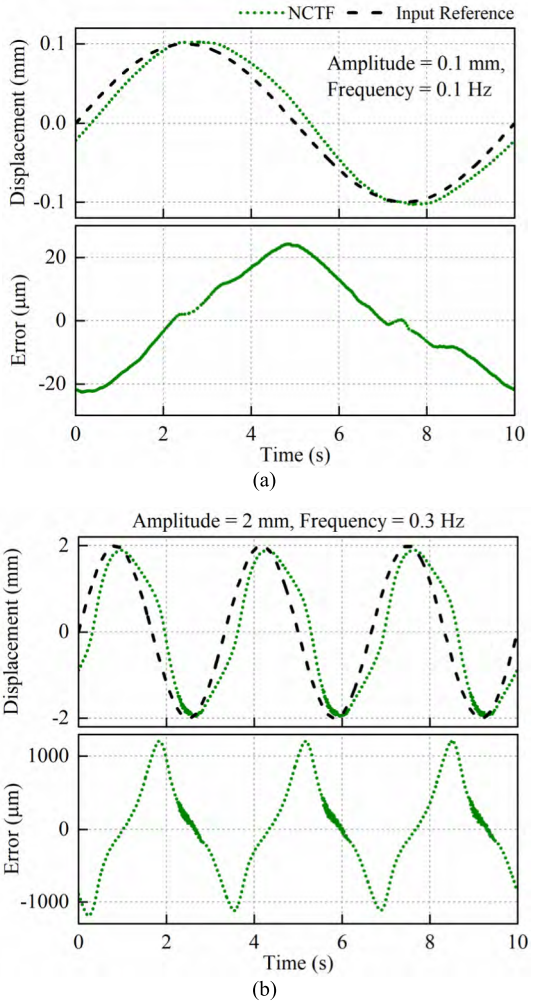

FIGURE 7. Experimental tracking performance of the conventional NCTF controller at (a) 0.1 mm and 0.1 Hz, and (b) 2 mm and 0.3 Hz.

insignificant to the input for the PI compensator, u_p. Moreover, the derivative element in the control structure will amplify the measurement noise that tends to result in the vibration. Therefore, it is more important to eliminate static deviation than reduce difference between the error rate of the NCT and the actual velocity in small working range. As a solution, the actual velocity feedback, $\dot{x}$ in the NCTF control structure has been removed in order to achieve requirement (A).

The low damping characteristic of the constructed PAM driven stage causes the mechanism tends to move easily, and results in large steady-state error that decreases accuracy of the motion control. To overcome this problem, an acceleration feedback compensator, K_a is included to the plant model. The acceleration feedback is expected to be able to increase the damping effect of the PAM mechanism and fulfill requirement (B). With the acceleration feedback compensator, the simplified first-order model of the PAM mechanism has been increased to second-order system as shown in (4).

$$G_{plant}(s) = \frac{k}{kK_a s^2 + \tau s + 1} \tag{4}$$

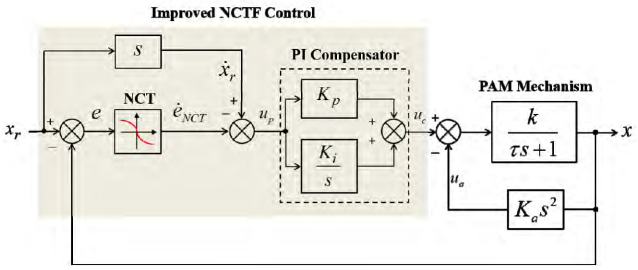

FIGURE 8. Control structure of the improved NCTF controller for the PAM mechanism. The actual velocity feedback is removed, and an acceleration feedback compensator and a reference rate feedforward are added based on the control structure of the conventional one.

Feedforward compensator is always useful to enhance the motion accuracy of a control system. In the improved NCTF control, the reference rate, $\dot{x}_r$ is added as the input signal to the PI compensator in order to satisfy requirement (C). In continuous motion, the reference rate, $\dot{x}_r$ is effective to increase the movement of the mechanism rapidly and thus enhance the following characteristic of the mechanism. The PAM

mechanism will perform small tracking error if it shows high following characteristics of its motion. The control law of the improved NCTF controller is formulated in (5). The constructed NCT of the conventional NCTF controller is adopted in the improved NCTF controller, while the PI compensator is required to redesign due to the changes of the control law. However, the controller design remains the simplicity of control structure and design procedure.

$$u_c(s) = (\dot{e}_{NCT}(s) + x_r(s)s)\left(K_p + \frac{K_i}{s}\right) \tag{5}$$

D. DESIGN PROCEDURE OF THE IMPROVED NCTF CONTROL SYSTEM

The design procedure of the improved NCTF controller comprises three major steps, which it can be designed based on the steps as follows:

1) CONSTRUCTION OF NCT

The NCT is constructed on the phase plane using the measured open-loop displacement and velocity responses during the deceleration motion. Fig. 9(a) presents the open-loop responses that are measured when the PAM mechanism is driven by a step input, u_r of 4 V (80% of the rated input to the actuator). The modified input signal is a combination of an exponential input and a step input, with the purpose to produce a smooth velocity response during the deceleration. As can be read in Fig. 9(a), the final displacement, x_f is 2.4 mm. Fig. 9(b) illustrates the constructed NCT, and the inclination at origin of the NCT is referred as β.

2) DESIGN OF PI COMPENSATOR

The PI compensator is designed experimentally using a practical stability limit. The practical stability limit is defined as the margin of stability, and it is obtained based on the information of the measured open-loop responses and the NCT which they are referred to the transfer function of the estimated plant model and the inclination of the NCT, respectively. Both parameters are used to derive the equation of practical stability limit. The PI gains are selected under the stable region of the practical stability limit using the actual mechanism.

Practical stability limit is found by driving the mechanism with the control structure as shown in Fig. 10. The value of K_p is increased until continuous oscillations at the steady-state in order to determine the proportional gain that indicates the existence of instability. Once the system is unstable, the gain is considered as actual ultimate proportional gain, K_{pu} (K_{pu} = 0.12 Vs/mm at 2 mm of the input reference). Based on the control structure in Fig. 10 with an integral gain, K_i, the closed-loop transfer function is expressed in (6).

$$\frac{X(s)}{X_r(s)} = \frac{\beta k K_p s + \beta k K_i}{\tau\left[s^2 + \left(\frac{\beta k K_p + 1}{\tau}\right)s + \frac{\beta k K_i}{\tau}\right]} \tag{6}$$

$$G_{closed-loop} = \frac{2\xi\omega_n s + \omega_n^2}{s^2 + 2\xi\omega_n s + \omega_n^2} \tag{7}$$

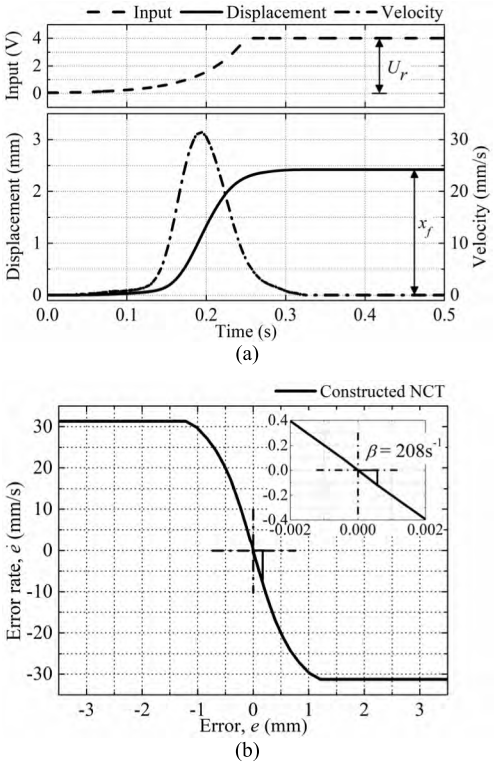

FIGURE 9. (a) Measured open-loop responses of the PAM mechanism, and (b) constructed NCT.

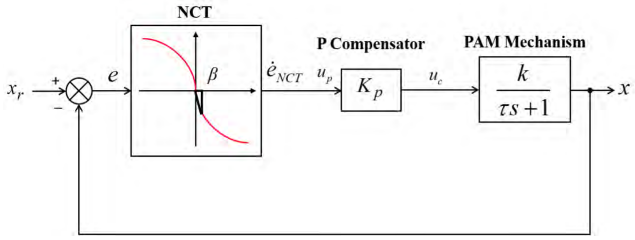

FIGURE 10. Control structure for designing the PI compensator.

By comparing the closed-loop transfer function to a second order system equation as shown in (7), the equations of proportional and integral compensator are derived as:

$$K_p = \frac{2\xi\omega_n\tau - 1}{\beta k} \tag{8}$$

$$K_i = \frac{\omega_n^2\tau}{\beta k} \tag{9}$$

Using the obtained K_{pu} and (8), the equation of practical stability, ξ_p can be expressed as shown in (10).

$$\xi_p = \frac{\beta k K_{pu} + 1}{2\omega_n\tau} \tag{10}$$

Fig. 11 illustrates the practical stability limit that shows the relationship between ξ and $\omega_n T_s$. The ξ and the ω_n that used to calculate PI compensator using (8) and (9), are selected from the stable region that bounded under the dashed line in Fig. 11. In order to ensure the designed PI compensator

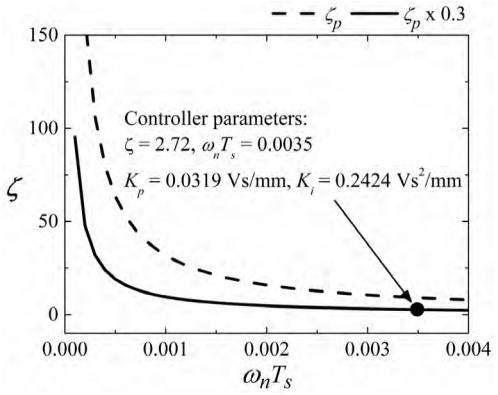

FIGURE 11. Practical stability limit (dashed line) and the controller compensation in respect to a safety margin of 70%(solid line).

is stable, it is selected further from the safety margin (area bounded under solid line). By examining experimentally, the PI gains at different safety margin with increment of 10% from the stability limit, the PI gains are eventually chosen at 70% of the safety margin. The PI compensator is chosen 30% of the values of ξ_p that calculated from (10). The use of high integral gain is used in this case to improve the positioning accuracy.

3) DETERMINATION OF ACCELERATION GAIN

The acceleration gain ($K_a = 1\times10^{-5}$ Vs^2/mm) is determined experimentally for sufficient damping characteristic.

The design procedure of the improved NCTF control for pneumatic artificial muscle actuated system remains as simple as the conventional NCTF control [39]. In the improved NCTF control, K_a is the only additional adjustable parameter. There are no extra experiments should be conducted to determine the control element. And, there are no any exact model parameters needed in the controller design.

E. STABILITY ANALYSIS OF THE IMPROVED NCTF CONTROL SYSTEM

The improved NCTF controller is experimentally designed under the stable condition. For further verification, the stability of the proposed controller is examined in detail. In general, the motion control of a mechanism is controlled by a digital controller. Thus, the discrete-time improved NCTF control system is used to analyze its stability.

Fig. 12 shows the discrete-time improved NCTF control system. Using backward difference rule, the pulse transfer function of the NCT, G_n(z), the PI compensator, G_c(z) and the PAM mechanism, G_o(z) are represented by (11)-(13). With (11)-(13), the pulse transfer function of the improved NCTF control system is obtained as stated in (14).

Based on (14), it proves that the coefficient of the pulse transfer function of the improved NCTF control system are functions of ξ, $\omega_n T_s$ and βT_s. This finding is useful to show that the stability of the controller is dependent on the ξ and ω_n. As the PI compensator is designed based on the ξ and

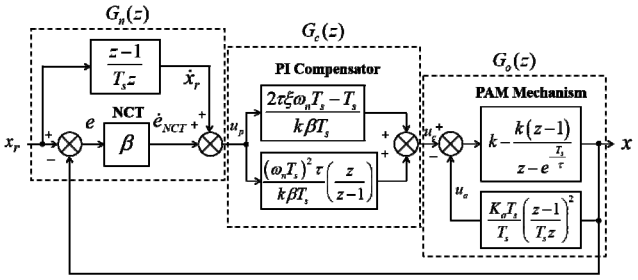

FIGURE 12. Discrete-time improved NCTF control system.

ω_n that bounded under stable region of the practical stability limit, therefore it expected that the practical stability limit is useful for the stability criterion of the control system.

$$G_n(z) = \frac{z-1}{T_s z} + \beta - \frac{\beta}{x_r} \tag{11}$$

$$G_c(z) = K_p + K_i\left(\frac{T_s z}{z-1}\right) = \frac{2\tau\xi\omega_n T_s - T_s}{k\beta T_s} + \frac{\tau\,(\omega_n T_s)^2}{k\beta T_s}\left(\frac{z}{z-1}\right) \tag{12}$$

$$\begin{aligned} G_o(z) &= \frac{kT_s^2 z^2\left(z - e^{-\frac{T_s}{\tau}}\right) - kT_s^2 z^2\,(z-1)}{T_s^2 z^2\left(z - e^{-\frac{T_s}{\tau}}\right) + kK_a\left(z - e^{-\frac{T_s}{\tau}}\right)(z-1)^2} \\ &\quad - kK_a\,(z-1)^3 \\ &\quad \times \begin{pmatrix} \mu_1\beta T_s + \mu_2\mu_3 + \mu_2\mu_5 + \mu_1 + \mu_3 T_s + \\ \mu_5 T_s - \mu_2 T_s - T_s^2 - \mu_1\mu_5\beta - \\ \mu_2\mu_3 e^{-\frac{T_s}{\tau}} - \mu_1 e^{-\frac{T_s}{\tau}} - \mu_3\mu_5 \end{pmatrix} z^4 \\ &\quad + \begin{pmatrix} \mu_2 T_s + \mu_1\mu_5\beta + 2T_s^2 + 2\mu_1 e^{-\frac{T_s}{\tau}} + \\ \mu_3\mu_5 - \mu_1\beta T_s - \mu_2\mu_5 - 2\mu_1 - \\ 2\mu_5 T_s - \mu_3 T_s \end{pmatrix} z^3 + \end{aligned} \tag{13}$$

$$\begin{aligned} \frac{X(z)}{X_r(z)} &= \frac{\left(\mu_1 + \mu_5 T_s - T_s^2 - \mu_1 e^{-\frac{T_s}{\tau}}\right) z^2}{\mu_2 T_s z^5 + \begin{pmatrix} \mu_4 T_s^3 + \mu_1\beta T_s + \mu_2\mu_3 - \mu_4 e^{-\frac{T_s}{\tau}} \\ -2\mu_2 T_s - \mu_1\mu_5\beta - \mu_2\mu_3 e^{-\frac{T_s}{\tau}} \end{pmatrix} z^4} \\ &\quad + \left(3\mu_4 e^{-\frac{T_s}{\tau}} + \mu_2 T_s + \mu_1\mu_5\beta - 3\mu_4 - \mu_1\beta T_s\right) z^3 \\ &\quad + \left(3\mu_4 - 3\mu_4 e^{-\frac{T_s}{\tau}}\right) z^2 + \left(\mu_4 e^{-\frac{T_s}{\tau}} - \mu_4\right) z \end{aligned} \tag{14}$$

where $\mu_1 = 2\tau\xi\omega_n T_s^2$; $\mu_2 = \beta T_s^2$; $\mu_3 = \tau\omega_n^2 T_s^2$; $\mu_4 = kK_a\beta T_s$; $\mu_5 = T_s e^{-\frac{T_s}{\tau}}$.

IV. EXPERIMENTAL RESULTS

In this section, the experimental point-to-point positioning and tracking performances of the PAM drive stage are examined. The conventional NCTF controller and classical PI

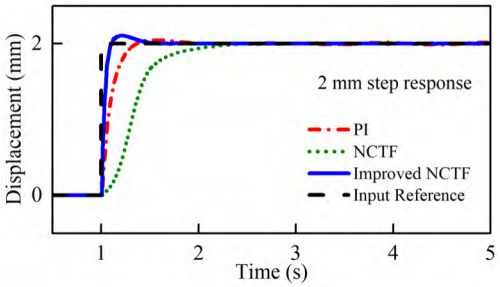

FIGURE 13. Step response comparison between the PI controller, the conventional NCTF controller and the improved NCTF controller at 2 mm of the tuning reference.

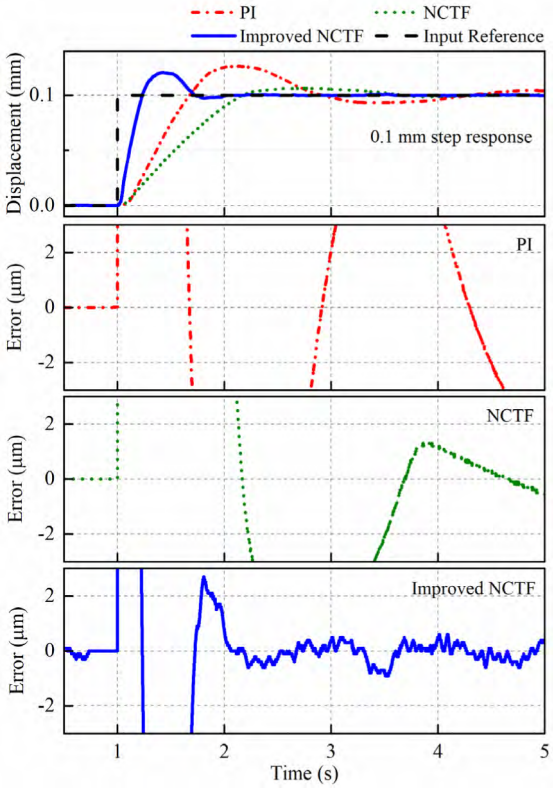

FIGURE 14. Experimental point-to-point positioning performance comparison: Desired (0.1 mm) and output responses (first), error of PI (second), error of NCTF (third), error of improved NCTF (fourth).

controller are used in the comparison in order to verify the effectiveness of the improved NCTF controller. Under the same input reference, the controllers are designed in order to achieve a comparable performance. Fig. 13 shows the optimum performance of the controllers, where the PI controller demonstrates slightly overshoot, and the conventional NCTF demonstrates no overshoot. The controller parameters of the controllers are summarized in Table 1.

Figs. 14 and 15 illustrate the experimental positioning performances of the PI controller, conventional NCTF controller, and improved NCTF controller at 0.1 mm and 1 mm of the step height, respectively. In positioning, the improved NCTF controller demonstrates much better performance than

TABLE 1. Controller parameters.

Controller	K_p	K_i	β	K_a
PI	0.4 V/mm	3.5 Vs/mm	-	-
NCTF	0.0142 Vs/mm	0.0384 Vs^2/mm	208 s^{-1}	-
Improved NCTF	0.0319 Vs/mm	0.2424 Vs^2/mm	208 s^{-1}	1 x 10^{-5} Vs^2/mm

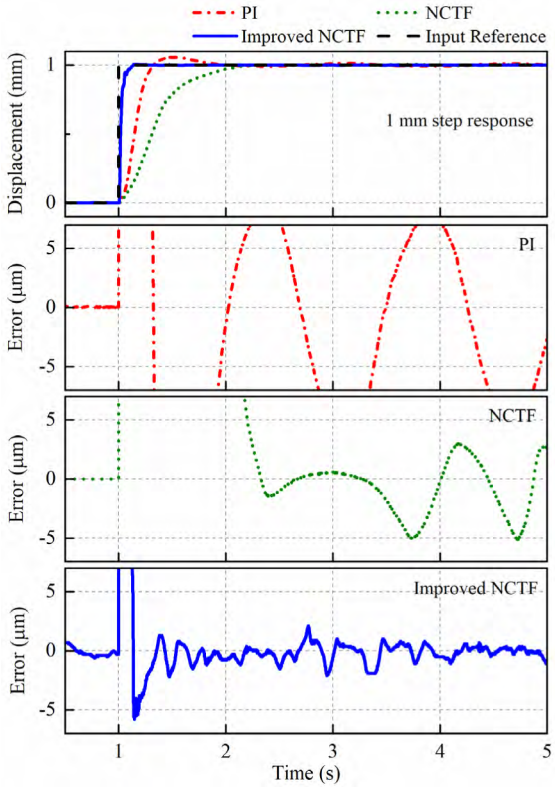

FIGURE 15. Experimental point-to-point positioning performance comparison: Desired (1 mm) and output responses (first), error of PI (second), error of NCTF (third), error of improved NCTF (fourth).

the PI controller and the conventional NCTF controller. The improved NCTF controller shows slightly overshoot, but it has significantly reduced the rise time, settling time, and steady-state error. Table 2 presents the quantitative results of 10 experiments for each controller in average and standard deviation. The improved NCTF controller demonstrates the positioning accuracy within 0.7 μm at 0.1 mm and 2.3 μm at 1 mm, which it shows 90% and 83% of the improvement in positioning accuracy as benchmarked to the PI controller respectively. As compared to the conventional NCTF controller, the improved NCTF controller shows 22% and 63% of the improvement in positioning accuracy at 0.1 mm and 1 mm respectively. The acceleration feedback compensator efficiently eliminates the oscillation and enhances the positioning accuracy of the PAM mechanism. The improved NCTF controller also demonstrates shorter rise time and settling time than both PI and conventional NCTF controllers. Due to the fast transient response, the improved NCTF controller exhibits a slightly high overshoot at 0.1 mm of the

TABLE 2. Average and standard deviation of 10 experiments for point-to-point positioning performance comparison.

Step height	Performance index	PI		NCTF		Improved NCTF	
		Avg.	Std. Dev.	Avg.	Std. Dev.	Avg.	Std. Dev.
0.1 mm	T_r (s)	0.45	4.2×10^{-3}	0.87	8.8×10^{-3}	0.17	4.8×10^{-3}
	T_s (s)	1.90	9.2×10^{-3}	2.48	2.2×10^{-2}	0.84	7.6×10^{-2}
	OS (%)	26.0	1.7×10^{-1}	5.5	3.0×10^{-1}	19.9	5.7×10^{-1}
	E_{ss} (μm)	6.8	9.2×10^{-2}	0.9	2.3×10^{-1}	0.7	1.4×10^{-1}
1.0 mm	T_r (s)	0.19	2.9×10^{-17}	0.61	4.7×10^{-3}	0.04	7.3×10^{-18}
	T_s (s)	0.81	2.3×10^{-16}	1.10	2.4×10^{-2}	0.12	5.3×10^{-3}
	OS (%)	5.5	6.0×10^{-2}	0	0	0	0
	E_{ss} (μm)	13.6	3.6×10^{-1}	6.2	7.4×10^{-1}	2.3	2.0×10^{-1}

T_r = rise time, T_s = settling time, OS = overshoot, E_{ss} = steady-state error

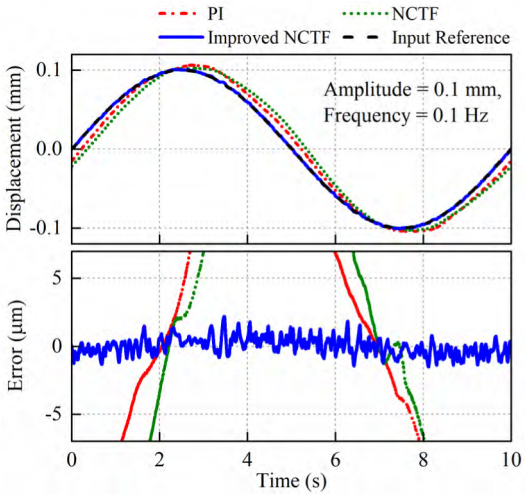

FIGURE 16. Experimental tracking performance comparison: Desired (0.1 Hz and 0.1 mm) and output responses (top), tracking errors (bottom).

small working range. However, the fast transient response has demonstrated its advantage in tracking performance, which will be discussed in the next paragraph.

Figs. 16 and 17 show the comparative tracking performances at different amplitudes (0.1 mm, 2 mm) of 0.1 Hz, while the comparative tracking performances of 0.3 Hz are showed in Figs. 18 and 19. Each experiment is performed in 6 cycles. Table 3 and 4 summarize the average and standard deviation of 10 experiments for tracking errors. The root mean square (RMS) error and the peak error are calculated based on the equations as follows:

$$\text{RMS error} = \sqrt{\frac{(x_{r1}-x_1)^2+(x_{r2}-x_2)^2+\ldots+(x_{rn}-x_n)^2}{n}} \tag{15}$$

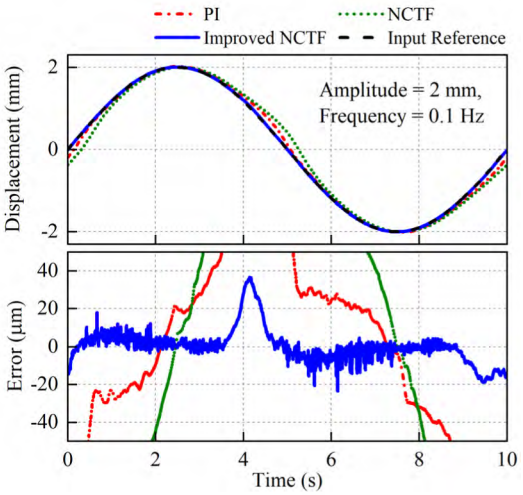

FIGURE 17. Experimental tracking performance comparison: Desired (0.1 Hz and 2 mm) and output responses (top), tracking errors (bottom).

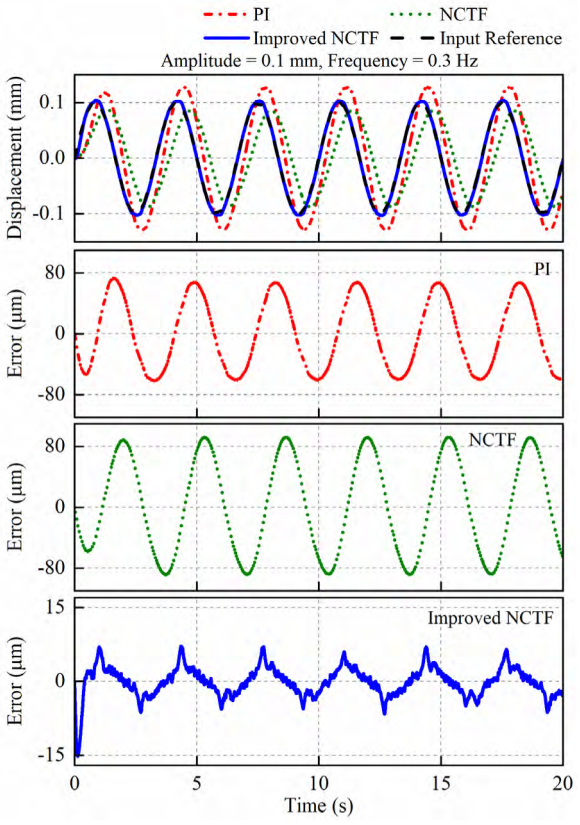

FIGURE 18. Experimental tracking performance comparison: Desired (0.3 Hz and 0.1 mm) and output responses (top), tracking errors (bottom).

$$\text{Peak error} = max\left(\sqrt{(x_r-x)^2_{min}}, \sqrt{(x_r-x)^2_{max}}\right) \tag{16}$$

Again, the improved NCTF controller shows much better tracking performance than both PI and conventional NCTF controllers, which the improved NCTF controller has significantly reduced the tracking errors of the system. As observed in Figs. 18 and 19, the improved NCTF controller shows a

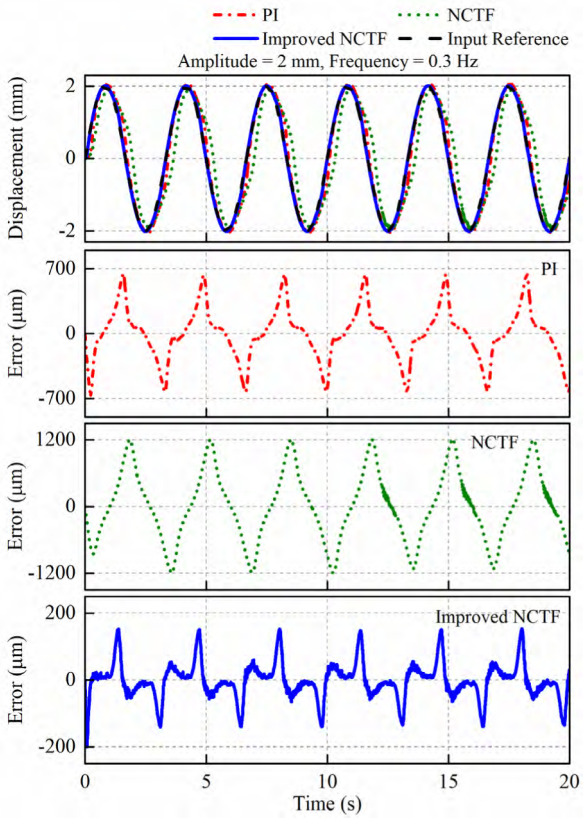

FIGURE 19. Experimental tracking performance comparison: Desired (0.3 Hz and 2 mm) and output responses (top), tracking errors (bottom).

good tracking performance in the high frequency as well for the small and large working range. Both PI and conventional NCTF controllers could not follow the motion at the frequency 0.3 Hz and amplitude 0.1 mm, and they show larger tracking error in the high frequency. At 0.3 Hz and 2 mm, the conventional NCTF controller exhibits the vibration. Based on the Table 3, the improved NCTF controller provides a consistency of tracking errors reduction in both low and high frequencies. In contrast to the PI controller, the improved NCTF controller improves RMS error about 92% at 0.1 Hz, and 88% at 0.3 Hz in average of all the amplitudes, while it improves peak error about 85% at 0.1 Hz, and 83% at 0.3 Hz. As compared to the conventional NCTF controller, the improved NCTF controller demonstrates higher percentage of improvement in tracking errors, which it improves about 95% in RMS error and 92% in peak error for all input references. The modified control structure in the improved NCTF controller successfully eliminates the vibration in the fast tracking motion. Also, the feedforward compensator efficiently improves the following characteristic. In contrast, the improved NCTF controller demonstrates better peak error reduction than the SMC that proposed in [17]. The peak error of the improved NCTF controller is 2.2% and 1.76% of the desired input at 0.1 mm and 2.0 mm for 0.1 Hz respectively.

Overall, it is clear to conclude that the improved NCTF controller has demonstrated a high positioning accuracy and

TABLE 3. Average and standard deviation of 10 experiments for tracking performance comparison in RMS error.

Input reference		Average of RMS error (μm)					
		PI		NCTF		Improved NCTF	
Freq. (Hz)	Amp. (mm)	Avg.	Std. Dev.	Avg.	Std. Dev.	Avg.	Std. Dev.
0.1	0.1	9.9	0.16	13.8	0.23	0.7	0.05
	2.0	88.3	0.43	185.4	0.85	9.0	0.15
0.3	0.1	48.1	0.96	63.9	0.17	2.9	0.18
	2.0	277.1	1.08	vibrate	-	53.0	0.21

TABLE 4. Average and standard deviation of 10 experiments for tracking performance comparison in peak error.

Input reference		Average of peak error (μm)					
		PI		NCTF		Improved NCTF	
Freq. (Hz)	Amp. (mm)	Avg.	Std. Dev.	Avg.	Std. Dev.	Avg.	Std. Dev.
0.1	0.1	15.0	0.31	23.1	0.61	2.2	0.11
	2.0	218.4	2.98	411.1	2.38	35.2	1.27
0.3	0.1	71.2	1.41	93.0	0.27	7.9	0.45
	2.0	639.1	1.84	vibrate	-	152.2	1.28

fast tracking performance at different working range. The advantage of the improved NCTF controller is that it has a simple design procedure without involving any exact model parameters, and yet it is able to show a high precision motion and fast positioning performance in both point-to-point positioning and continuous motion.

V. CONCLUSION

In the present paper, a simple and practical control strategy has been proposed for the point-to-point positioning and tracking motions of the PAM drive stage, while the robust and stability performances are assured too. The improved NCTF controller has been designed and improved based on the conventional NCTF controller, in order to overcome the vibration problem in fast tracking motion, and low following characteristic. Based on the conventional NCTF control structure, the actual velocity feedback is removed in order to eliminate the static deviation. To overcome the low damping characteristic of the PAM mechanism, the acceleration feedback compensator is added. The acceleration feedback compensator is successfully eliminated the oscillation and enhanced the positioning accuracy. Furthermore, the reference rate feedforward is included to the input of the PI compensator as the objective to increase the movement pace of the mechanism and improve the tracking performance in continuous motion. The improved NCTF remains the simple design procedure as the conventional one. The effectiveness of the proposed controller was evaluated experimentally, and the performances were compared with the PI controller and the conventional NCTF controller. The experimental results indicate that the improved NCTF controller has achieved better performances than both PI and conventional NCTF

controllers in both point-to-point and continuous motions. Overall, the improved NCTF controller has showed the capability in performing high precision motion and promising results for the PAM mechanism.

ACKNOWLEDGMENT

The authors would like to acknowledge Centre for Robotics and Industrial Automation, Universiti Teknikal Malaysia Melaka and Motion Control Research Laboratory for the laboratory facilities and equipment support.

REFERENCES

[1] B. Tondu and P. Lopez, "Modeling and control of McKibben artificial muscle robot actuators," *IEEE Control Syst.*, vol. 20, no. 2, pp. 15–38, Apr. 2000.

[2] R. A. R. C. Gopura, D. S. V. Bandara, K. Kiguchi, and G. K. I. Mann, "Developments in hardware systems of active upper-limb exoskeleton robots: A review," *Robot. Auton. Syst.*, vol. 75, pp. 203–220, Jan. 2016.

[3] S. Hussain, S. Q. Xie, and P. K. Jamwal, "Adaptive impedance control of a robotic orthosis for gait rehabilitation," *IEEE Trans. Cybern.*, vol. 43, no. 3, pp. 1025–1034, Jun. 2013.

[4] Y.-L. Park, B.-R. Chen, N. O. Pérez-Arancibia, D. Young, L. Stirling, R. J. Wood, E. C. Goldfield, and R. Nagpal, "Design and control of a bio-inspired soft wearable robotic device for ankle–foot rehabilitation," *Bioinspiration Biomimetics*, vol. 9, no. 1, p. 16007, 2014.

[5] Z. Wong, C. Teng, and Y. Z. Chong, "Power assisted pnumatic-based knee-ankle-foot-orthosis for rehabilitation," in *Proc. IEEE-EMBS Conf. Biomed. Eng. Sci.*, Malaysia, Dec. 2012, pp. 300–304.

[6] K. Hosoda, Y. Sakaguchi, H. Takayama, and T. Takuma, "Pneumatic-driven jumping robot with anthropomorphic muscular skeleton structure," *Auton. Robots*, vol. 28, no. 3, pp. 307–316, Apr. 2010.

[7] J. Lei and J. Zhu, "Pneumatic artificial muscles force modelling and the position and stiffness control on the knee joint of the musculoskeletal leg," *Int. J. Bioautomat.*, vol. 21, no. 1, pp. 31–42, 2017.

[8] M. Li, X. Wang, W. Guo, P. Wang, and L. Sun, "System design of a cheetah robot toward ultra-high speed," *Int. J. Adv. Robot. Syst.*, vol. 11, no. 5, p. 73, May 2014.

[9] R. Niiyama, S. Nishikawa, and Y. Kuniyoshi, "Athlete robot with applied human muscle activation patterns for bipedal running," in *Proc. 10th IEEE-RAS Int. Conf. Humanoid Robots*, Dec. 2010, pp. 498–503.

[10] Y. Yamada, S. Nishikawa, K. Shida, R. Niiyama, and Y. Kuniyoshi, "Neural-body coupling for emergent locomotion: A musculoskeletal quadruped robot with spinobulbar model," in *Proc. IEEE/RSJ Int. Conf. Intell. Robots Syst.*, Sep. 2011, pp. 1499–1506.

[11] S. Chakravarthy, K. Aditya, and A. Ghosal, "Development of miniaturized pneumatic artificial muscle for surgical device," in *Proc. 1st Int. 16th Nat. Conf. Mach. Mech.*, 2013, pp. 339–345.

[12] T. Deaconescu and A. Deaconescu, "Pneumatic muscle-actuated adjustable compliant gripper system for assembly operations," *J. Mech. Eng.*, vol. 63, no. 4, pp. 225–234, 2017.

[13] P. Ohta, L. Valle, J. King, K. Low, J. Yi, C. G. Atkeson, and Y.-L. Park, "Design of a lightweight soft robotic arm using pneumatic artificial muscles and inflatable sleeves," *Soft Robot.*, vol. 5, no. 2, pp. 204–215, Apr. 2018.

[14] L. Hao, H. Yang, Z. Sun, C. Xiang, and B. Xue, "Modeling and compensation control of asymmetric hysteresis in a pneumatic artificial muscle," *J. Intell. Mater. Syst. Struct.*, vol. 28, no. 19, pp. 2769–2780, Mar. 2017.

[15] F. Schreiber, Y. Sklyarenko, K. Schlüter, J. Schmitt, S. Rost, A. Raatz, and W. Schumacher, "Tracking control with hysteresis compensation for manipulator segments driven by pneumatic artificial muscles," in *Proc. IEEE Int. Conf. Robot. Biomimetics*, Phuket, Thailand, Dec. 2011, pp. 2750–2755.

[16] H. Aschemann and D. Schindele, "Sliding-mode control of a high-speed linear axis driven by pneumatic muscle actuators," *IEEE Trans. Ind. Electron.*, vol. 55, no. 11, pp. 3855–3864, Nov. 2008.

[17] D. X. Ba and K. K. Ahn, "Indirect sliding mode control based on grey-box identification method for pneumatic artificial muscle," *Mechatronics*, vol. 32, pp. 1–11, Dec. 2015.

[18] J. Cao, S. Q. Xie, and R. Das, "MIMO sliding mode controller for gait exoskeleton driven by pneumatic muscles," *IEEE Trans. Control Syst. Technol.*, vol. 26, no. 1, pp. 274–281, Jan. 2017.

[19] K. Xing, Q. Xu, J. Huang, Y. Wang, J. He, and J. Wu, "Tracking control of pneumatic artificial muscle actuators based on sliding mode and non-linear disturbance observer," *IET Control Theory Appl.*, vol. 4, no. 10, pp. 2058–2070, Oct. 2010.

[20] P. Carbonell, Z. P. Jiang, and D. W. Repperger, "Nonlinear control of a pneumatic muscle actuator: Backstepping vs. Sliding-mode," in *Proc. IEEE Int. Conf. Control Appl.*, Mexico City, Mexico, Sep. 2001, pp. 167–172.

[21] D. Schindele and H. Aschemann, "Nonlinear model predictive control of a fast parallel robot actuated by pneumatic muscles," *IFAC Proc.*, vol. 40, no. 12, pp. 591–596, 2007.

[22] L. Zhang, J. Xie, and D. Lu, "Adaptive robust control of one-link joint actuated by pneumatic artificial muscles," in *Proc. 1st Int. Conf. Bioinformat. Biomed. Eng.*, 2007, pp. 1185–1189.

[23] G. Andrikopoulos, G. Nikolakopoulos, and S. Manesis, "Pneumatic artificial muscles: A switching model predictive control approach," *Control Eng. Pract.*, vol. 21, no. 12, pp. 1653–1664, Dec. 2013.

[24] D. W. Repperger, K. R. Johnson, and C. A. Phillips, "A VSC position tracking system involving a large scale pneumatic muscle actuator," in *Proc. 37th IEEE Conf. Decis. Control*, vol. 4, Dec. 1998, pp. 4302–4307.

[25] G. Andrikopoulos, G. Nikolakopoulos, and S. Manesis, "Advanced nonlinear PID-based antagonistic control for pneumatic muscle actuators," *IEEE Trans. Ind. Electron.*, vol. 61, no. 12, pp. 6926–6937, Dec. 2014.

[26] H. P. H. Anh, "Online tuning gain scheduling MIMO neural PID control of the 2-axes pneumatic artificial muscle (PAM) robot arm," *Expert Syst. Appl.*, vol. 37, no. 9, pp. 6547–6560, Sep. 2010.

[27] S. W. Chan, J. H. Lilly, D. W. Repperger, and J. E. Berlin, "Fuzzy PD+I learning control for a pneumatic muscle," in *Proc. 12th IEEE Int. Conf. Fuzzy Syst.*, St. Louis, MO, USA, vol. 1, May 2003, pp. 278–283.

[28] M.-K. Chang, "An adaptive self-organizing fuzzy sliding mode controller for a 2-DOF rehabilitation robot actuated by pneumatic muscle actuators," *Control Eng. Pract.*, vol. 18, no. 1, pp. 13–22, 2010.

[29] M.-K. Chang, "Adaptive self-tuning fuzzy controller for a soft rehabilitation machine actuated by pneumatic artificial muscles," *Open J. Appl. Sci.*, vol. 5, no. 5, pp. 199–211, 2015.

[30] A. Rezoug, B. Tondu, M. Hamerlain, and M. Tadjine, "Adaptive fuzzy nonsingular terminal sliding mode controller for robot manipulator actuated by pneumatic artificial muscles," in *Proc. IEEE Int. Conf. Robot. Biomimetics*, Dec. 2013, pp. 334–339.

[31] L. D. Khoa, D. Q. Truong, and K. K. Ahn, "Synchronization controller for a 3-R planar parallel pneumatic artificial muscle (PAM) robot using modified ANFIS algorithm," *Mechatronics*, vol. 23, no. 4, pp. 462–479, Jun. 2013.

[32] M. Chandrapal, X. Chen, W. Wang, and C. Hann, "Nonparametric control algorithms for a pneumatic artificial muscle," *Expert Syst. Appl.*, vol. 39, no. 10, pp. 8636–8644, Aug. 2012.

[33] B. K. S. Woods and Y. Choi, "Control system development for pneumatic artificial muscle-driven active rotor systems," *J. Guid., Control, Dyn.*, vol. 36, no. 4, pp. 1177–1185, 2013.

[34] S.-H. Chong and K. Sato, "Nominal characteristics trajectory following control as practical controller: A review," in *Proc. 41st Annu. Conf. IEEE Ind. Electron. Soc. (IECON)*, Nov. 2015, pp. 004790–004795.

[35] G. J. Maeda and K. Sato, "Practical control method for ultra-precision positioning using a ballscrew mechanism," *Precis. Eng.*, vol. 32, no. 4, pp. 309–318, Oct. 2008.

[36] R. M. Nor and S. H. Chong, "Continuous motion NCTF control of a one mass rotary system," in *Proc. IEEE Int. Conf. Control Syst., Comput. Eng.*, Malaysia, Sep. 2013, pp. 316–321.

[37] K. Sato and G. J. Maeda, "A practical control method for precision motion—Improvement of NCTF control method for continuous motion control," *Precis. Eng.*, vol. 33, no. 2, pp. 175–186, Apr. 2009.

[38] K. Sato, K. Nakamoto, and A. Shimokohbe, "Practical control of precision positioning mechanism with friction," *Precis. Eng.*, vol. 28, no. 4, pp. 426–434, Oct. 2004.

[39] A. Wahyudi, K. Sato, and A. Shimokohbe, "Robustness evaluation of three friction compensation methods for point-to-point (PTP) positioning systems," *Robot. Auton. Syst.*, vol. 52, nos. 2–3, pp. 247–256, Aug. 2005.

[40] S.-H. Chong and K. Sato, "Practical controller design for precision positioning, independent of friction characteristic," *Precis. Eng.*, vol. 34, no. 2, pp. 286–300, Apr. 2010.

[41] S. H. Chong, H. Hashimoto, and K. Sato, "Practical motion control with acceleration reference for precision motion—New NCTF control and its application to non-contact mechanism," *Precis. Eng.*, vol. 35, no. 1, pp. 12–23, 2011.
[42] S. H. Chong and K. Sato, "Practical and robust control for precision motion: AR-CM NCTF control of a linear motion mechanism with friction characteristics," *IET Control Theory Appl.*, vol. 9, no. 5, pp. 745–754, Mar. 2015.
[43] K. Sato and Y. Sano, "Practical and intuitive controller design method for precision positioning of a pneumatic cylinder actuator stage," *Precis. Eng.*, vol. 38, no. 4, pp. 703–710, Oct. 2014.

T. F. TANG received the B.Eng. and M.Sc. degrees in manufacturing engineering from the Universiti Teknikal Malaysia Melaka (UTeM), Malaysia, in 2012 and 2015, respectively. He is currently pursuing the Ph.D. degree in electrical engineering from the Universiti Teknikal Malaysia Melaka (UTeM), Malaysia. His research interests include motion control, actuators, mechatronics, and system design and control.

S.-H. CHONG received the B.Eng. and M.Sc. degrees in electrical engineering from the Universiti Teknologi Malaysia (UTM), Malaysia, in 2001 and 2003, respectively, and the D.Eng. degree in mechano-micro engineering from the Tokyo Institute of Technology (Tokyo Tech), Japan, in 2010. She is currently an Associate Professor with the Department of Control, Instrumentation, and Automation, Faculty of Electrical Engineering, Universiti Teknikal Malaysia Melaka (UTeM). Her research interests include motion control, smart manufacturing IR4.0, mechatronic systems design and modelling, precision engineering, and rehabilitation systems. She is the Founding Member and Secretary of Malaysian Society of Automatic and Control Engineers (MACE) – IFAC NMO. She is the member of IFAC Technical Committee Control Design (IFAC TC 2.1), and Mechatronics (IFAC TC 4.2), too.

R. MOHD NOR was born in Miri, Sarawak, on May 27, 1988. She received the first B.Eng. degree in electrical engineering (control, instrumentation, and automation), in 2011, and the M.Sc. degree in electrical engineering from Universiti Teknikal Malaysia Melaka, 2015. She is currently a Lecturer with the Faculty of Electrical and Electronic Engineering Technology, Universiti Teknikal Malaysia Melaka. Her major field of study is in control system design and application. She is a member of Board of Engineers Malaysia (BEM) and Malaysian Board of Technologist (MBOT).

KAIJI SATO received the B.Eng., M.Eng., and D. Eng. degrees from the Tokyo Institute of Technology (Tokyo Tech), Tokyo, Japan, in 1987, 1989, and 1995, respectively. He is currently a Professor with the Department of Mechanical Engineering, Toyohashi University of Technology. His research interests include electromagnetic/electrostatic actuators, precision mechanisms, precision motion control, micro-dynamics of mechatronics systems, micromachines, and microelectromechanical systems.